

# Bandwidth-controlled Mott transition in $\kappa$ -(BEDT-TTF)<sub>2</sub>Cu[N(CN)<sub>2</sub>]Br<sub>x</sub>Cl<sub>1-x</sub>:

## I. Optical studies of localized charge excitations

Daniel Faltermeier, Jakob Barz, Michael Dumm, Natalia Drichko,\* and Martin Dressel†  
*1. Physikalisches Institut, Universität Stuttgart, Pfaffenwaldring 57, D-70550 Stuttgart Germany*

Cécile Meziere and Patrick Batail  
*Laboratoire CIMI, FRE 2447 CNRS-Université d'Angers, Bât. K,  
 UFR Sciences, 2 Bd. Lavoisier, F-49045 Angers, France*  
 (Dated: February 8, 2020)

Infrared reflection measurements of the half-filled two-dimensional organic conductors  $\kappa$ -(BEDT-TTF)<sub>2</sub>Cu[N(CN)<sub>2</sub>]Br<sub>x</sub>Cl<sub>1-x</sub> were performed as a function of temperature (5 K  $< T <$  300 K) and Br-substitution ( $x = 0\%$ , 40%, 73%, 85%, and 90%) in order to study the metal-insulator transition. We can distinguish absorption processes due to itinerant and localized charge carriers. The broad mid-infrared absorption has two contributions: transitions between the two Hubbard bands and intradimer transitions from the charges localized on the (BEDT-TTF)<sub>2</sub> dimer. Since the latter couple to intramolecular vibrations of BEDT-TTF, the analysis of both electronic and vibrational features provides a tool to disentangle these contributions and to follow their temperature and electronic-correlations dependence.

PACS numbers: 71.10.Hf, 71.30.+h, 74.25.Gz, 74.70.Kn

### I. INTRODUCTION

The physics of strongly correlated electron systems is a very active field in solid-state science where the vicinity of Mott-insulating, magnetically ordered, and superconducting ground states is most intriguing. These effects are intensively studied for transition-metal oxides, in particular high-temperature superconductors, and organic conductors. It is extremely interesting that all of these materials show a similar competition between ordered antiferromagnetic and superconducting phases: this suggests common physics, while the chemistry of the compounds and the origin of the conducting electrons is different.<sup>1,2,3</sup> These facts have initiated our investigation of the molecular conductors of the BEDT-TTF family as model compounds to study physics of correlated electrons close to the Mott transition in two dimensions.<sup>4,5</sup>

In the  $\kappa$ -phase crystals, conducting layers of cationic bis-(ethylenedithio)tetrathiafulvalene (BEDT-TTF) molecules are separated by ‘charge-reservoir’ layers of monovalent anions. As depicted in Fig. 1, the BEDT-TTF<sup>+0.5</sup> molecules form confacial dimers which can be considered as lattice sites; due to this dimerization the conduction band is half filled. The anion size sensitively influences the physical properties of the system very similar to the variation of pressure, since they define the spacing between the molecules (molecular sites) and thus the width of the band.<sup>6,7</sup> The ratio of electronic correlations to the width of the conductance band is the control parameter<sup>3</sup> in the phase diagram depicted in Fig. 2. The ground state of  $\kappa$ -(BEDT-TTF)<sub>2</sub>X salts can be switched between an antiferromagnetic insulating, a superconducting, and a metallic state. They exhibit the highest superconducting transition temperature of all organic superconductors with  $T_c = 12.5$  K.<sup>1,2</sup>

At ambient temperature the  $\kappa$ -phase BEDT-TTF salts

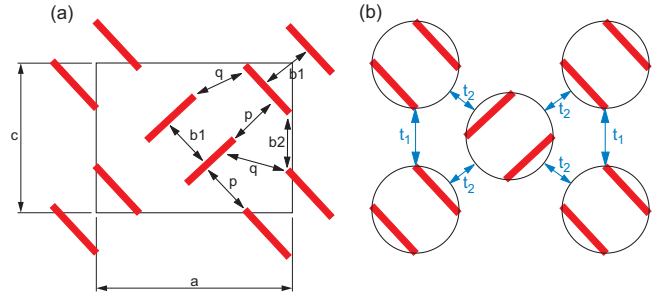


FIG. 1: (a) Structural arrangement of the BEDT-TTF molecules in the  $\kappa$ -phase (looking along the molecular axes); the size of the unit cell is approximately 12.9 Å in  $a$ -direction, 8.5 Å along the  $c$  axis, and 30.0 Å in the third direction. The overlap integrals are labelled according to Mori *et al.* (Ref. 6). The interdimer overlap integral  $b1$  is around 0.027, along the dimer chains  $b2 \approx 0.010$ , while  $p$  and  $q$  link orthogonal molecules with approximately 0.011 and 0.004, respectively. (b) Triangular lattice for the dimer model of  $\kappa$ -(BEDT-TTF)<sub>2</sub>X. There is hopping in along the stacks  $t_1$  and along the diagonals  $t_2$ .

of our study have common properties, which may be characterized as a narrow-gap semiconductor or ‘bad metal’. When the temperature drops below a so-called coherence temperature  $T_{coh} \approx 50$  K on the right side of the phase diagram, the metallic behavior becomes dominant due to the formation of Fermi liquid quasiparticles<sup>8,9</sup> until a second-order transition occurs to a superconducting state. The nature of superconductivity in organic crystals is subject to discussion for twenty years<sup>10</sup> but in the present study we focus on the metallic and insulating states. On the left side of the phase diagram (Fig. 2), i.e., for higher values of  $U/t$ , the system never shows metallic properties, but is gradually driven into an insulating state

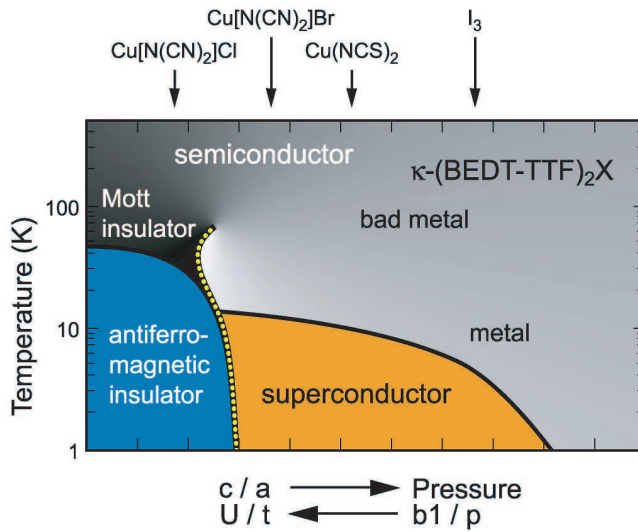


FIG. 2: Schematic phase diagram of the  $\kappa$ -phase salts  $(\text{BEDT-TTF})_2X$ . Instead of tuning the external pressure, the same ambient-pressure ground state can be achieved by modifying the anions  $X$ . The arrows indicate the approximate position of  $\kappa-(\text{BEDT-TTF})_2\text{Cu}[\text{N}(\text{CN})_2]\text{Cl}$ ,  $\kappa-(\text{BEDT-TTF})_2\text{Cu}[\text{N}(\text{CN})_2]\text{Br}$ ,  $\kappa-(\text{BEDT-TTF})_2\text{Cu}(\text{NCS})_2$ , and  $\kappa-(\text{BEDT-TTF})_2\text{I}_3$  at ambient pressure, respectively. The phase transition between the (antiferromagnetic) Mott insulator and the metal/superconductor can be explored by gradually replacing Cl by Br in  $\kappa-(\text{BEDT-TTF})_2\text{Cu}[\text{N}(\text{CN})_2]\text{Br}_x\text{Cl}_{1-x}$ .  $c$  and  $a$  are the lattice parameters;  $b_1$  and  $p$  indicate the transfer integral according to Fig. 1.  $U/t$  is the on-site Coulomb repulsion with respect to the hopping integral  $t$ .

by electronic correlations as the temperature drops below 90 K; at  $T_N \approx 35$  K magnetic order is observed. NMR measurements in deuterated samples (which fall right on the phase boundary) revealed that at low temperatures the transition between the commensurate antiferromagnet and pseudogapped superconductor is of first order.<sup>11</sup> Most recently, huge research efforts were dedicated to the metal-to-insulator transition and critical end-point in this highly correlated two-dimensional electron system. The critical behavior in the vicinity of the Mott transition was investigated by dc measurements under external pressure and in magnetic field.<sup>12,13,14</sup> The alloyed series  $\kappa-(\text{BEDT-TTF})_2\text{Cu}[\text{N}(\text{CN})_2]\text{Br}_x\text{Cl}_{1-x}$ , studied in the present work, covers the most interesting region of the phase diagram spanned by the pure Cl and Br salts, including the border between the Mott insulating and metallic phases. Our infrared reflection measurements of a series of compounds with Br concentration  $x$  varying between 0 and 90 % make it possible to explore the temperature and correlation (bandwidth)-dependent charge dynamics on crossing this phase boundary, as well as the unusual physical properties in the metallic region above the superconducting transition.

Several optical experiments were performed on the pristine compounds  $\kappa-(\text{BEDT-TTF})_2\text{Cu}[\text{N}(\text{CN})_2]\text{Br}$  and  $\kappa-(\text{BEDT-TTF})_2\text{Cu}[\text{N}(\text{CN})_2]\text{Cl}$  over

the years.<sup>15,16,17,18,19,20,21</sup> They gave a general idea of the electronic excitation observed in the infrared region: a broad mid-infrared band around  $2500 - 3500 \text{ cm}^{-1}$  and a narrow Drude-like peak in the spectra of superconducting Br-compound<sup>22</sup> at temperatures below 50 K. In the discussion section IV we review the different interpretations of the mid-infrared spectra. Our investigation of the alloys gives an unambiguous assignment of the spectral features in this region, important for the analysis of the charge dynamics in these salts.  $\text{BEDT-TTF})_2\text{Cu}[\text{N}(\text{CN})_2]\text{Br}_{0.5}\text{Cl}_{0.5}$  is the only mixed compound which has been previously investigated by infrared spectroscopy,<sup>19,23,24,25,26</sup> but only in the mid-infrared range.

Here, we present for the first time a systematic optical study of the series  $\kappa-(\text{BEDT-TTF})_2\text{Cu}[\text{N}(\text{CN})_2]\text{Br}_x\text{Cl}_{1-x}$ , with  $x$  crossing all relevant regions of the phase diagram from the insulating/antiferromagnetic to the metallic/superconducting state. Our experiments cover a broad spectral range from 50 to  $10000 \text{ cm}^{-1}$  and temperatures from room temperature down to  $T = 5$  K. This enables us to follow the response of the free and localized carriers for the different points of this phase diagram, depending on temperature and correlation-to-bandwidth ratio. While we focus on the signature of localized charge excitations here, the succeeding paper<sup>27</sup> (which we refer to as Part II in the following) is devoted to the dynamics of free charge carriers and the formation of the coherent quasiparticle response.

## II. EXPERIMENTS

Single crystals of the  $\kappa-(\text{BEDT-TTF})_2\text{Cu}[\text{N}(\text{CN})_2]\text{Br}_x\text{Cl}_{1-x}$  salts were grown by standard electrochemical methods. Certain ratios of Br/Cl concentration were chosen to obtain a series of alloys. Subsequent to the optical reflection experiments, each individual crystal was checked by microprobe analysis in order to determine the composition. The actual Br/Cl ratio turned out to be significantly different than expected from the starting concentration, even varying within one batch. It was hardly possible to produce samples with predefined Br concentration. In the following, we denote the actual Br content of  $\kappa-(\text{BEDT-TTF})_2\text{Cu}[\text{N}(\text{CN})_2]\text{Br}_x\text{Cl}_{1-x}$  where  $x = 0\%$ ,  $40\%$ ,  $73\%$ ,  $85\%$ , and  $90\%$ ; the concentration was found homogeneous for each specimen. The platelets contained naturally flat  $a$ - $c$  surfaces with a typical size of about  $1 \times 1 \text{ mm}^2$ . The orientation was determined from the optical spectra.

The strong dependence of the dc resistivity on the Br/Cl ratio is emphasized in Fig. 3 where  $\rho(T)$  is plotted for a crystal with low ( $x = 23\%$ ) and high ( $x = 85\%$ ) bromine content. For the insulating sample  $\kappa-(\text{BEDT-TTF})_2\text{Cu}[\text{N}(\text{CN})_2]\text{Br}_{0.23}\text{Cl}_{0.77}$  the resistivity rises by many orders of magnitude as the temperature decreases, most dramatically below 70 K or so. Contrary,  $\kappa-(\text{BEDT-TTF})_2\text{Cu}[\text{N}(\text{CN})_2]\text{Br}_{0.85}\text{Cl}_{0.15}$  shows basically

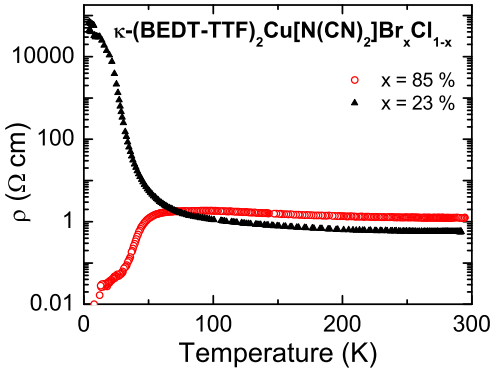


FIG. 3: Dc resistivity *versus* temperature of  $\kappa$ -(BEDT-TTF)<sub>2</sub>Cu[N(CN)<sub>2</sub>]Br<sub>0.23</sub>Cl<sub>0.77</sub> and  $\kappa$ -(BEDT-TTF)<sub>2</sub>Cu[N(CN)<sub>2</sub>]Br<sub>0.85</sub>Cl<sub>0.15</sub>.

the same temperature dependence like the pure Br specimen:  $\rho(T)$  increases slightly below room temperature until it reaches a broad maximum around 100 K. At lower temperatures the behavior is metallic with  $\rho(T) \propto T^2$  for  $T < 35$  K and finally a superconducting transition is observed at  $T_c \approx 12$  K.<sup>28</sup> The superconducting properties of  $\kappa$ -(BEDT-TTF)<sub>2</sub>Cu[N(CN)<sub>2</sub>]Br<sub>x</sub>Cl<sub>1-x</sub> with different Br concentrations have been investigated previously by dc resistivity and magnetization.<sup>32</sup>

The optical reflection was measured with light polarized along *a* and *c* axes, respectively. Employing a modified Bruker IFS 113v Fourier-transform spectrometer, we covered a broad frequency range from 50 to 10 000 cm<sup>-1</sup> (6 meV - 1.2 eV) with a resolution of up to 0.5 cm<sup>-1</sup>. The single crystals were studied at 300, 150, 90, 50, 35, 20 and 5 K with the help of a cold-finger cryostat. To achieve good thermal contact, the samples were fixed by carbon paste on a brass cone directly attached to the cold finger. Absolute values of the reflectivity are obtained by subsequently evaporating gold onto the sample and remeasuring it as reference mirror at all temperatures.<sup>33</sup> The *in-situ* gold-evaporation technique is more accurate than other referencing methods because it utilizes the entire sample surface and is less effected by surface imperfections. From the reflectivity spectra, the optical conductivity was calculated using Kramers-Kronig analysis.<sup>34</sup> The extrapolation to high frequencies used data on the related compound published by Drozdova *et al.*<sup>24</sup> At low-frequencies the data were extrapolated by the Hagen-Rubens behavior, which was double-checked by the dc resistivity obtained from standard four-probe measurements (Fig. 3). Although the absolute values of the ac conductivity are very sensitive to the extrapolation, the main features in the measured region and important physics communicated in this and the second part are not affected.

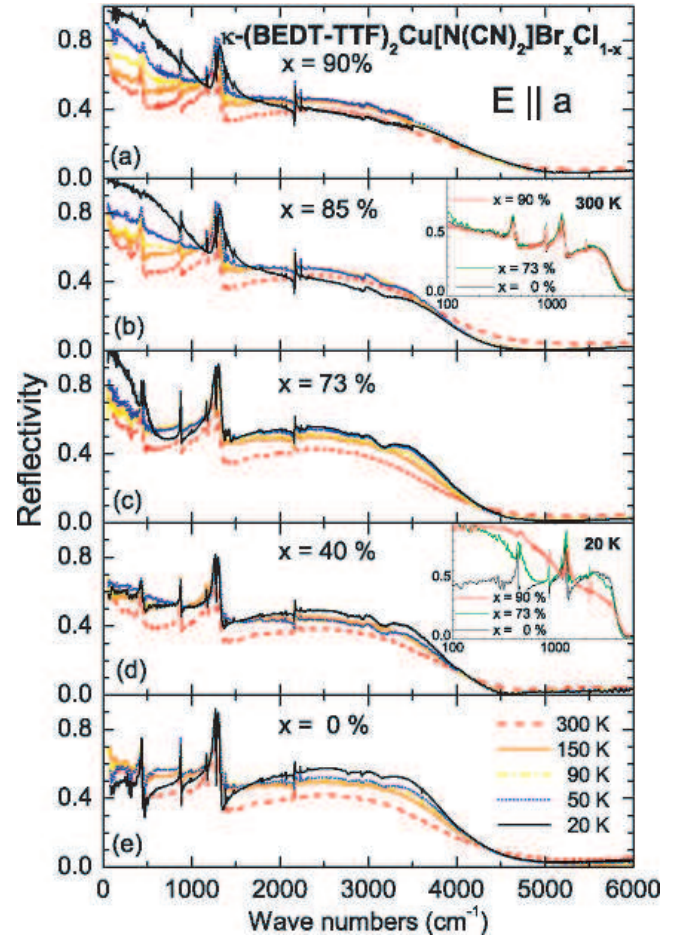


FIG. 4: Reflectivity spectra of  $\kappa$ -(BEDT-TTF)<sub>2</sub>Cu[N(CN)<sub>2</sub>]Br<sub>x</sub>Cl<sub>1-x</sub> for the polarization  $E \parallel a$  measured at various temperatures:  $T = 300$  K, 150 K, 90 K, 50 K, and 20 K. The panels (a) - (e) correspond to different Br concentrations:  $x = 90\%$ , 85%, 73%, 40%, and 0%. The insets show the room-temperature and low-temperature spectra for  $x = 90\%$ , 73%, and 0% on a logarithmic frequency scale.

### III. RESULTS

In Figs. 4 and 5 the reflectivity and conductivity spectra of  $\kappa$ -(BEDT-TTF)<sub>2</sub>Cu[N(CN)<sub>2</sub>]Br<sub>x</sub>Cl<sub>1-x</sub> (with  $x = 0\%$ , 40%, 73%, 85%, and 90%) are displayed for light polarized parallel to the *a* direction at distinct temperatures from 300 K down to 20 K. Because there is no significant difference between the  $T = 20$  K and 5 K spectra, we omitted the latter. At ambient temperature, the optical properties only weakly depend on the Br-content (inset of Fig. 4b). As expected for semiconductors, the reflectivity is basically frequency independent at low frequencies, and hence the corresponding room-temperature conductivity is small; the reflectivity starts to decrease significantly above 3500 cm<sup>-1</sup> and reaches a value close to zero in both polarizations around 5000 cm<sup>-1</sup>. The respective conductivity spectra show a broad absorption feature centered between 2000 cm<sup>-1</sup> and 3000 cm<sup>-1</sup> which is well docu-

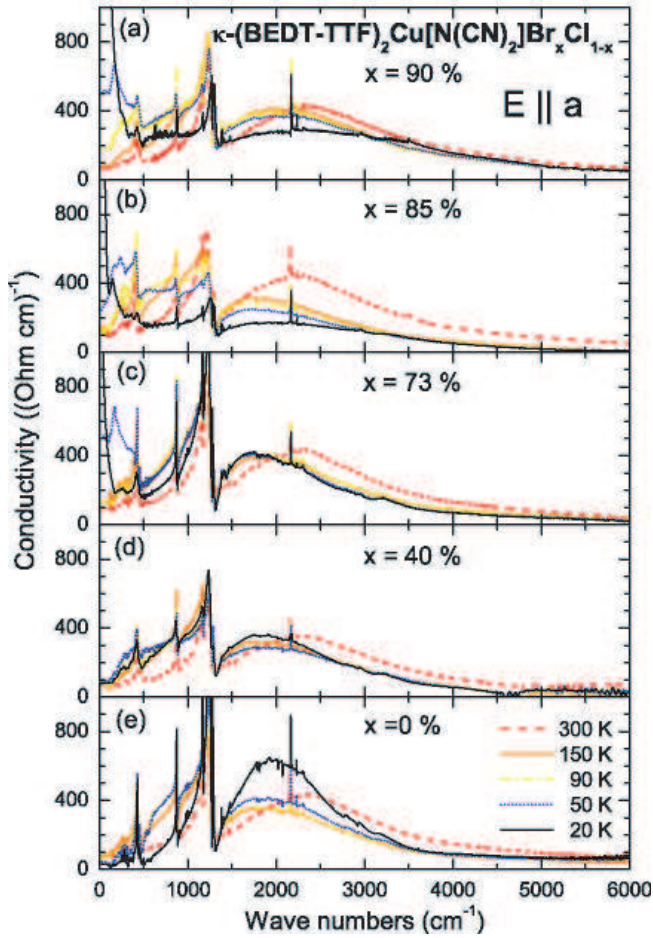


FIG. 5: Optical conductivity spectra ( $E \parallel a$ ) of  $\kappa$ -(BEDT-TTF)<sub>2</sub>Cu[N(CN)<sub>2</sub>]Br<sub>x</sub>Cl<sub>1-x</sub> at different Br concentrations  $x$  and temperatures.

mented in literature for the  $\kappa$ -phase of BEDT-TTF salts in general.

The strong phonon modes observed in the mid-infrared around 400, 850, and 1400 cm<sup>-1</sup> are totally symmetric vibrations of the BEDT-TTF molecule, activated by electron-molecular vibrational (emv) coupling (cf. Ref. 5 and references therein), while the narrow band at 2200 cm<sup>-1</sup> is a CN-stretching vibration of the anion. In the course of numerous vibrational studies on the  $\kappa$ -phase BEDT-TTF salts, Eldridge's group<sup>18,35,36,37</sup> and others<sup>20,24</sup> presented a complete assignment of the totally-symmetric vibrations. Here we use the C<sub>2h</sub> symmetry assignment which takes a deformation of a BEDT-TTF molecule inside the crystal into account.<sup>38</sup>

Significant changes of the optical behavior are observed when cooling the samples below  $T = 90$  K. The far-infrared reflectivity strongly increases for specimens with high Br content (Fig. 4), while the mid-infrared reflectivity is suppressed. Correspondingly, as plotted in Fig. 5 a Drude-like contribution develops in the conductivity spectra of the samples with  $x = 73\%$ , 85%, and 90% at low temperatures. The lat-

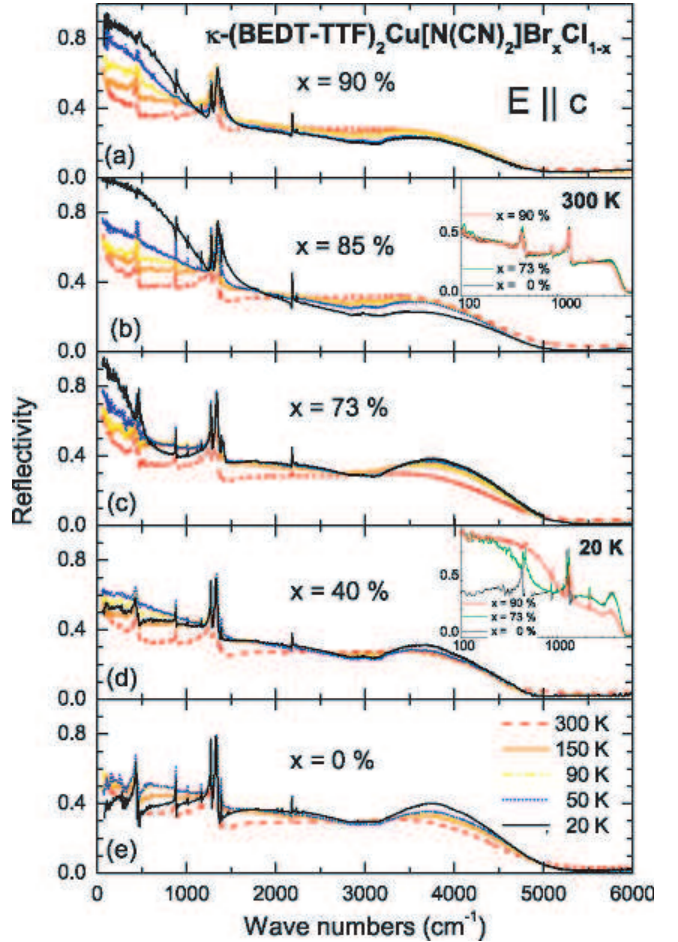


FIG. 6: Reflectivity spectra of  $\kappa$ -(BEDT-TTF)<sub>2</sub>Cu[N(CN)<sub>2</sub>]Br<sub>x</sub>Cl<sub>1-x</sub> for light polarized  $E \parallel c$  measured at various temperatures as indicated. The different panels (a) - (e) correspond to Br concentrations:  $x = 90\%$ , 85%, 73%, 40%, and 0%. The insets show the room-temperature and low-temperature spectra on a logarithmic frequency scale.

ter compound exhibits a behavior similar to the pristine  $\kappa$ -(BEDT-TTF)<sub>2</sub>Cu[N(CN)<sub>2</sub>]Br salt.<sup>15</sup> The opposite is observed for the salts with low Br-content: the far-infrared reflectivity decreases while it increases in the mid-infrared. The absolute values of reflectivity and conductivity are slightly enhanced compared to previously published results.<sup>15,17,18,19,20,21</sup> This we attribute to our advanced *in-situ* gold-evaporation method for the reference measurement which also accounts for imperfections of the crystal surface.

The reflectivity and conductivity for the perpendicular polarization ( $E \parallel c$ ) are shown in Figs. 6 and 7 for different Br concentrations  $x$  and temperatures  $T$ . The spectra exhibit basically the same features as the ones recorded along  $a$  direction; except the shape of the mid-infrared absorption is different. As previously reported, for most other  $\kappa$ -salts, the maximum of the absorption band for the  $c$  axis lies at higher frequencies. While at ambient temperature a distinction is difficult, at low tem-

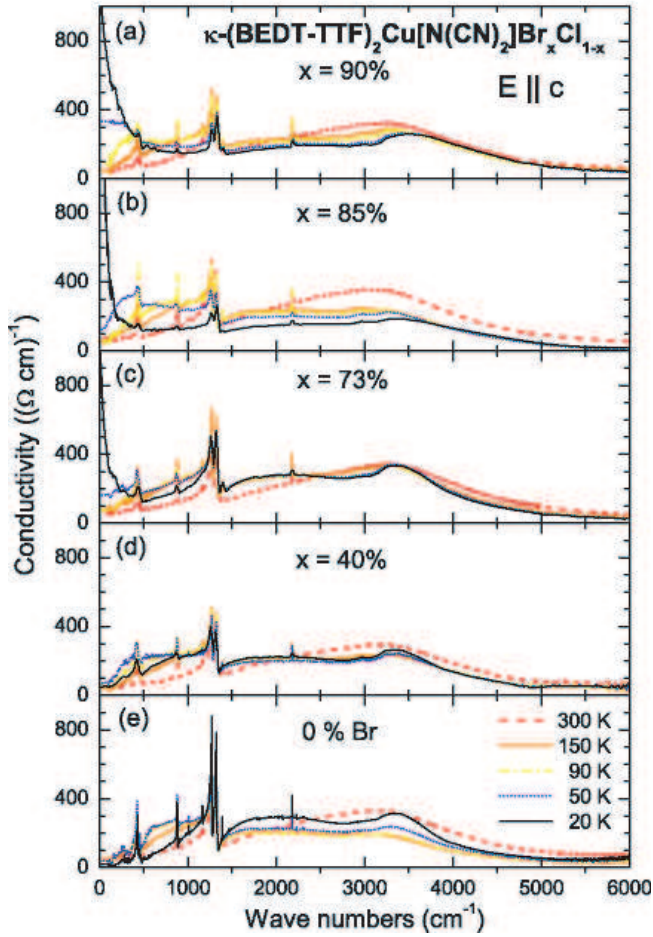


FIG. 7: Optical conductivity spectra ( $E \parallel c$ ) for  $\kappa$ -(BEDT-TTF)<sub>2</sub>Cu[N(CN)<sub>2</sub>]Br<sub>x</sub>Cl<sub>1-x</sub> of different Br concentrations (a)  $x = 90\%$ , (b)  $85\%$ , (c)  $73\%$ , (d)  $40\%$ , and (e)  $0\%$  measured at various temperatures:  $T = 300$  K,  $150$  K,  $90$  K,  $50$  K, and  $20$  K. The mid-infrared band clearly has two contributions.

peratures it becomes obvious from both, reflectivity and conductivity data that it consists of two components: in addition to the band around  $2000\text{ cm}^{-1}$  a second narrower mode has its maximum around  $3500\text{ cm}^{-1}$ . This behavior is most pronounced for the pure Cl compound. Again, with increasing Br content a Drude contribution develops as the temperature is reduced below  $50$  K.

We want to point out that the accessible frequency range of our experiments is limited to  $\nu \geq 50\text{ cm}^{-1}$  due to the small sample surfaces. Thus, we cannot detect the superconducting energy gap  $\Delta_0$ , which is expected around  $2\Delta_0 = 3.53k_B T_c \approx 30\text{ cm}^{-1}$ .

#### IV. DISCUSSION

Despite the above mentioned limitations, our data cover a very broad frequency range from  $50$  to  $10\,000\text{ cm}^{-1}$ . Therefore, we are able not only to study the vibrational features and the mid-infrared absorption,

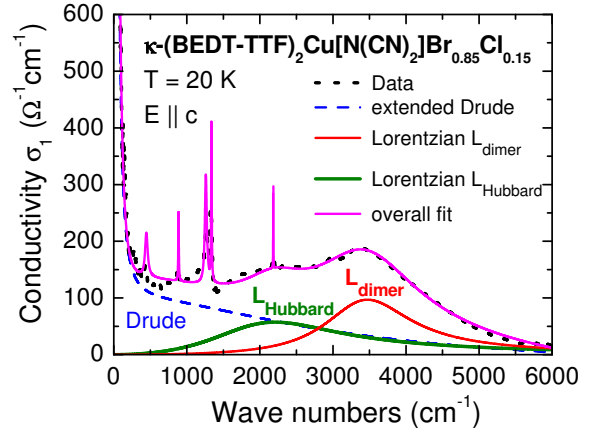


FIG. 8: Fit of the frequency dependent conductivity of  $\kappa$ -(BEDT-TTF)<sub>2</sub>Cu[N(CN)<sub>2</sub>]Br<sub>0.85</sub>Cl<sub>0.15</sub> at  $20$  K for the electric field polarized parallel to the  $c$  axis.  $L_{\text{dimer}}$  and  $L_{\text{Hubbard}}$  show the two Lorentz oscillators required to fit the mid-infrared peak. Five Lorentzians describe the phonon peaks. In addition an extended Drude model is included for the low-frequency increase.

but also to analyze the temperature and doping dependence of the Drude contribution in  $\kappa$ -(BEDT-TTF)<sub>2</sub>Cu[N(CN)<sub>2</sub>]Br<sub>x</sub>Cl<sub>1-x</sub>. However, since there is no agreement in the literature on the interpretation of the mid-infrared absorption band which is important for analysis of the whole charge dynamics in these materials, we first address this part of the spectra. The contribution of the itinerant electrons will be analyzed and discussed in Part II.

The common approach is to fit the spectra by the Drude-Lorentz model,<sup>5,34</sup> because it helps to disentangle the contributions of conduction electrons, interband transitions and phonons. As an example, the optical conductivity along the  $c$ -direction of the crystal with  $x = 0.85$  is displayed in Fig. 8 together with a fit by one Drude component and several Lorentzian oscillators; to put additional restrictions on the parameters, the  $R(\omega)$  and  $\sigma(\omega)$  spectra were fitted simultaneously. It was applied to the spectra in both polarizations and at all temperatures and values of Br doping.

##### A. Mid-Infrared band: overview of the different interpretations

The most prominent feature in the optical conductivity spectra of  $\kappa$ -phase BEDT-TTF salts, in general, is the broad mid-infrared hump. It peaks around  $2200\text{ cm}^{-1}$  for the polarization  $E \parallel a$  and at  $3200\text{ cm}^{-1}$  in the  $c$  direction, for which it shows a more complicated double structure. Although it becomes obvious – in particular when cooling down – that two contributions add up for this band, the explanations proposed over the years took into account only one isolated process. It was suggested that the mid-infrared peak is due to charge

transfer inside the dimer<sup>15,16,17,35,44</sup> or due to transitions between the Hubbard bands formed by the correlated conduction electrons.<sup>21,45,46</sup> Our present investigation on the substitution series  $\kappa$ -(BEDT-TTF)<sub>2</sub>Cu[N(CN)<sub>2</sub>]Br<sub>x</sub>Cl<sub>1-x</sub> sheds new light on this issue because it allows us to follow the features when going from metallic to insulating phase both by changing temperature  $T$  and by changing the relative correlation strength  $U/t$ .

Eldridge and coworkers<sup>15,17</sup> first suggested that the mid-infrared peak is due to charge-transfer bands, with the excitation confined to the dimers and the charge transfer occurring between adjacent molecules. The polarization dependence is explained by different interactions between neighboring dimers (Fig. 1a). The arguments were supported by electronic band-structure calculations of the  $\kappa$ -phase salts performed by Whangbo and collaborators on the basis of the tight-binding approximation.<sup>47,48</sup> The highest occupied band is half filled with only very little difference in bandwidth and density of states at the Fermi level when going from  $\kappa$ -(BEDT-TTF)<sub>2</sub>Cu[N(CN)<sub>2</sub>]Cl to  $\kappa$ -(BEDT-TTF)<sub>2</sub>Cu[N(CN)<sub>2</sub>]Br. Obviously this is a very rough approximation which cannot even explain both the semiconducting behavior at ambient temperature, and a redistribution of the spectral weight from this mid-infrared maximum to the Drude-peak for compounds with high Br concentration on cooling (discussed in Part II), or the difference in the ground states of the compounds.

A more consistent picture was reached, when both components of the optical conductivity, the Drude-like contribution and the mid-infrared hump were explained in the framework of a half-filled two-dimensional system with strong electronic correlations.<sup>6,49</sup> The structure of the  $\kappa$  phase was mapped on an anisotropic triangular lattice, each site presenting one dimer as depicted in Fig. 1b. The intradimer overlap plays the role of the effective on-site Coulomb interaction  $U_{\text{eff}}$ .<sup>6,49,50</sup> Consequently,  $U_{\text{eff}}$  increases with dimerization: for the Cl-analog b1 is slightly higher which causes larger  $U_{\text{eff}}$ . *Ab-initio* calculations by Fortunelli and Painelli give the value of  $U_{\text{eff}} = 0.4$  eV for a dimer in  $\kappa$ -(BEDT-TTF)<sub>2</sub>Cu[N(CN)<sub>2</sub>]Br; this is in agreement with experiments.<sup>51</sup>

The interdimer overlap integrals define the hopping  $t$  between the sites considered by theory. Following the suggestion by Fukuyama and collaborators<sup>4,49</sup> we can map the structure to a triangular half-filled lattice with transfer integrals  $t_1 = 30$  meV and  $t_2 = 50$  meV. It has been predicted by theory that the Mott-insulator transition in a two-dimensional lattice typically occurs when  $U$  is comparable to the bandwidth  $W = 8t$ . In the present case  $U_{\text{eff}}/t \approx 8$ ; implying that we are very close to the metal-insulator transition.  $U_{\text{eff}}/t$  increases on going from Br to Cl anions, i.e. on moving from right to left in the phase diagram (Fig. 2) and leads to localization of the charge carriers.<sup>52</sup> Following these considerations, recently<sup>21</sup> the experimentally observed mid-infrared band was associated with the transition between the Hubbard bands at  $\hbar\omega \approx U_{\text{eff}}$ , i.e. around 3000 cm<sup>-1</sup>.

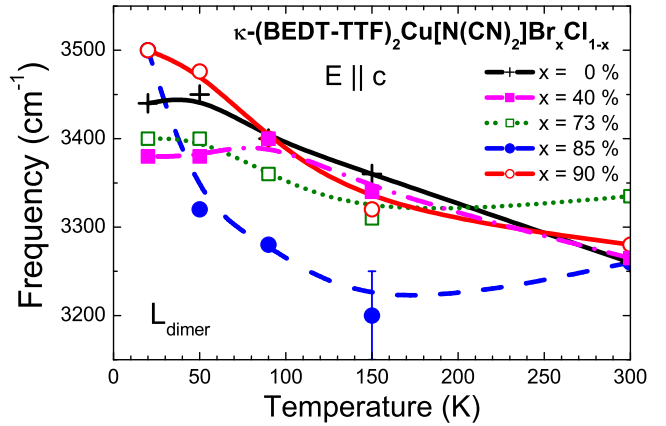


FIG. 9: Temperature dependence of the mid-infrared peak  $L_{\text{dimer}}$  in  $\kappa$ -(BEDT-TTF)<sub>2</sub>Cu[N(CN)<sub>2</sub>]Br<sub>x</sub>Cl<sub>1-x</sub> with  $x = 0\%$ , 40%, 73%, 85%, and 90% obtained by a Lorentzian fit for the polarization  $E \parallel c$ . The lines are guides to the eye.

A treatment of the metallic side of the phase diagram by dynamical mean-field theory<sup>9,46</sup> proposes, that besides the mid-infrared band around  $U_{\text{eff}}$ , a quasiparticle peak at the Fermi level grows with temperature below  $T_{\text{coh}} \approx 0.1t^*$ , where  $t^*$  is the overlap integral. Due to transition between the coherent quasiparticle band and the Hubbard bands, a new peak is supposed to develop around  $\hbar\omega \approx U_{\text{eff}}/2$  for  $T < T_{\text{coh}}$ .

Our interpretation of the optical spectra takes into account both types of contribution. From our analysis we can disentangle the component coming from charge transfer inside the dimers and the interdimer processes which can be described by a Hubbard model. We propose that the interdimer transition cause the high-frequency contribution  $L_{\text{dimer}}$ , while the band  $L_{\text{Hubbard}}$  at lower frequencies is ascribed to the transition between the Hubbard bands.

## B. Excitations localized on dimers: charge transfer and emv-coupled features

The narrow high-frequency peak  $L_{\text{dimer}}$  with a maximum around 3200 cm<sup>-1</sup> can be clearly distinguished in the polarization  $E \parallel c$ ; in contrast, our fit for  $E \parallel a$  shows that in the  $a$  direction it is hidden under the  $L_{\text{Hubbard}}$  mode and cannot be extracted reliably. This anisotropy of the spectra in the mid-infrared range is well documented for these  $\kappa$  salts.<sup>5,53</sup>

Within the uncertainty of the Lorentz fit, at ambient temperature the position of the high-frequency oscillator  $L_{\text{dimer}}$  is independent of Br content; also the oscillator strength of this band does not vary substantially. The temperature dependence of the  $L_{\text{dimer}}$  frequency ( $E \parallel c$ ) is plotted in Fig. 9 for different Br concentrations. In general there is an upward shift of approximately 100 to 200 cm<sup>-1</sup> when going down to  $T = 20$  K; it is due to the thermal contraction. The difference between metallic and

insulating compounds is seen at 50 K and lower: while the temperature dependent high-frequency shift of  $L_{\text{dimer}}$  accelerates upon cooling in the more metallic samples with  $x = 90\%$  and  $85\%$ , for the insulating ones with low Br concentration it levels off. Obviously the  $L_{\text{dimer}}$  oscillator frequency is not related to the effects which occur to the conduction electrons: although the Mott-Hubbard energy gap opens for the insulating samples at  $T \leq 50$  K, the  $L_{\text{dimer}}$  excitation is observed at smaller frequencies than for the metallic compounds. At low temperatures, the  $L_{\text{dimer}}$  mode is broader for the metals with high Br concentration compared to the insulating Cl-rich compounds; most probably due to the interaction with the conduction electrons.

When comparing the  $L_{\text{dimer}}$  oscillator and the emv-coupled vibrational features, a very similar temperature and concentration dependence becomes obvious; it helps to improve the interpretation of the mid-infrared spectra. The most prominent  $\nu_4(A_g)$  vibration involves a symmetric stretching of the C=C double bonds;<sup>54</sup> at room temperatures it is observed at about  $1240\text{ cm}^{-1}$  along the  $a$ -axis and at  $1280\text{ cm}^{-1}$  along the  $c$ -axis in the spectra of the  $\kappa$ -(BEDT-TTF)<sub>2</sub>Cu[N(CN)<sub>2</sub>]Br<sub>x</sub>Cl<sub>1-x</sub>. We estimate the center frequency of the  $\nu_4(A_g)$  band by fitting it with a Lorentzian, disregarding the anti-resonances due to  $\nu_6(A_g)$  mode for a moment. As can be seen from Fig. 11a and c, with decreasing temperature ( $300\text{ K} \leq T < 50\text{ K}$ ) the  $\nu_4(A_g)$  modes slightly shift to higher frequencies in about the same manner for all compounds. As  $T$  is reduced this tendency enhances further for  $x = 85\%$  and  $90\%$ : the total shift amounts to approximately  $45\text{ cm}^{-1}$  for  $E \parallel a$ , and less than  $5\text{ cm}^{-1}$  in  $c$  direction; the variation saturates at very low temperatures. For the insulating compounds with low Br content, the  $\nu_4(A_g)$  mode even reverses its temperature dependence below  $T_{\text{coh}} \approx 50\text{ K}$  and becomes softer. Except some gradual difference, the behavior is very similar for both orientations. Below 50 K, the  $\nu_4(A_g)$  mode becomes sharper in the insulating samples while it widens and seems to be weaker for high Br content.

The  $\nu_6(A_g)$  mode (a vibration of the CH<sub>2</sub> groups), which for  $E \parallel a$  has a frequency in the range of this wide maximum, is seen in Fig. 10 as an antiresonance around  $1270$  to  $1280\text{ cm}^{-1}$ . At low temperatures four bands of  $\nu_6(A_g)$  are resolved, due to the four distinct CH<sub>2</sub> groups per unit cell. We follow the temperature dependence by choosing the minimum around  $1273\text{ cm}^{-1}$ . Again, for low Br content the  $\nu_6(A_g)$  mode gradually moves down in frequency with decreasing temperature, while it significantly shifts to higher values for  $x = 85\%$  and  $90\%$ , as displayed in Fig. 11c. The same temperature dependence of  $\nu_6(A_g)$  is observed parallel to  $c$  (Fig. 11d).

The similar temperature and Br-concentration dependence is seen for the peaks of the emv-coupled ‘ring-breathing’ mode  $\nu_{10}(A_g)$  of the BEDT-TTF molecule<sup>43</sup> at  $870\text{ cm}^{-1}$  and  $885\text{ cm}^{-1}$  and of the  $\nu_{13}(A_g)$  at about  $430\text{ cm}^{-1}$ . Accordingly, the peaks are pretty intense in the insulating state, and are less significant in the

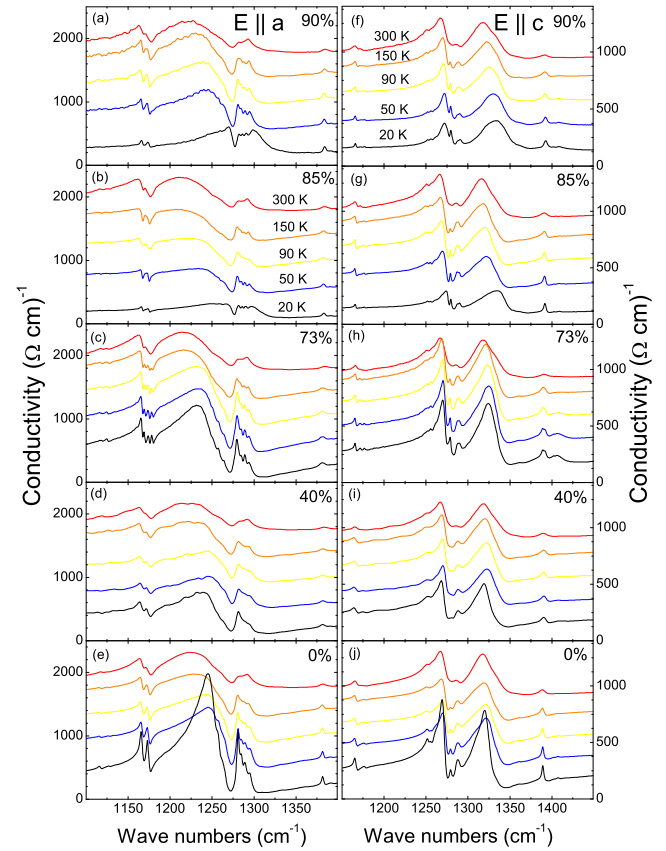


FIG. 10: Detailed view of the optical conductivity of  $\kappa$ -(BEDT-TTF)<sub>2</sub>Cu[N(CN)<sub>2</sub>]Br<sub>x</sub>Cl<sub>1-x</sub> along the  $a$  and  $c$ -directions (left and right panels, respectively) for different Br concentrations  $x = 90\%$ ,  $85\%$ ,  $73\%$ ,  $40\%$ , and  $0\%$ , (a)-(e) and (f)-(j), respectively. The spectra for the different temperatures (bottom to top:  $T = 20\text{ K}$ ,  $50\text{ K}$ ,  $90\text{ K}$ ,  $150\text{ K}$ , and  $300\text{ K}$ ) are offset by  $400\text{ }(\Omega\text{cm})^{-1}$  for clarity.

spectra for high Br concentration. On the other hand, the infrared active modes, both the  $\nu_{45}(B_{2u})$  vibration of BEDT-TTF molecule detected around  $1383\text{ cm}^{-1}$  (Fig. 10) and CN-stretch vibration of the anion layer observed around  $2160\text{ cm}^{-1}$  do not depend on the Br-concentration and show only the expected hardening with temperature decrease.

The cluster model of M.J. Rice<sup>55</sup> and Yartsev<sup>56,57</sup> showed that due to emv coupling to the charge-transfer excitation the vibrational modes become infrared active but are shifted down to lower frequencies with respect to the corresponding Raman modes. A simple consideration for emv-coupling in a dimer<sup>57</sup> demonstrates that when the charge transfer band shifts down in frequencies, the low-frequency displacement of the coupled features increases. The simplest case of a charge transfer in a dimer gives sufficient intensity to the emv-coupled features<sup>56</sup> and it qualitatively describes this contribution to the  $\kappa$ -phase spectra.

Since the average amount of charge per BEDT-TTF molecule ( $+0.5e$ ) remains constant, the upward-shift of

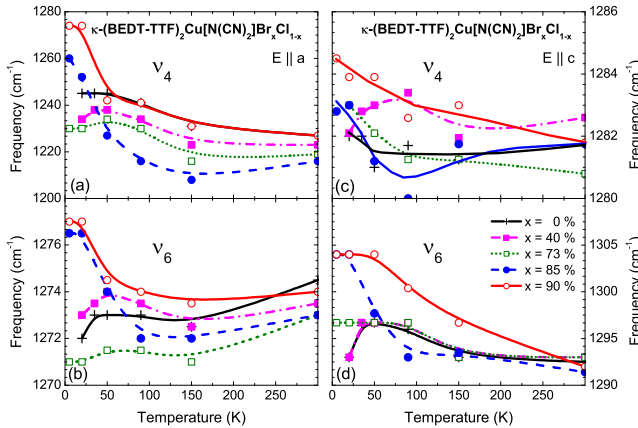


FIG. 11: Temperature dependence of the mode frequencies of the intramolecular vibrations  $\nu_4(A_g)$  and  $\nu_6(A_g)$  for  $\kappa$ -(BEDT-TTF)<sub>2</sub>Cu[N(CN)<sub>2</sub>]Br<sub>x</sub>Cl<sub>1-x</sub>. (a) The  $\nu_4(A_g)$  mode along the  $a$ -direction was fitted by a Lorentzian and the center frequency plotted. (b) In the case of  $\nu_6(A_g)$  the frequencies are defined as the minima in the respective optical conductivity, i.e. the strongest of the quadrupole. In frames (c) and (d) the equivalent data are presented for the polarization  $E \parallel c$ . The lines correspond to spline fits.

the center frequency of the emv-coupled modes indicates the respective change in the electronic transition to which they are coupled. The positions of the vibrational features follow the  $L_{\text{dimer}}$  oscillator (Fig. 9) and the shape of the features is also correlated. This suggests the assignment of the  $L_{\text{dimer}}$  oscillator to the charge transfer between the molecules in a dimer, which activates the emv-coupling. Although  $L_{\text{dimer}}$  and  $L_{\text{Hubbard}}$  are hard to distinguish for in the  $a$  direction, it is obvious that the  $L_{\text{dimer}}$  mode is located at much lower frequencies (around 2600 cm<sup>-1</sup>) and that it is weaker than for  $E \parallel c$ . In general the charge transfer band between the molecules is expected to shift up in energy when the overlap between the molecules becomes stronger. This implies that the band of the intradimer transition lies at higher frequencies than the transition between the dimers.<sup>58</sup> The same result is received by the cluster model, when it is extended to tetramers and hexamers; the electronic transitions which sums up the intradimer and interdimer excitations shift to lower frequencies and gets wider. This confirms our interpretation of the optical spectra. The present assignment also explains the in-plane anisotropy of the emv-coupled features, which follows the anisotropy of the  $L_{\text{dimer}}$  peak, i.e., all emv coupled modes are softer along  $a$  axis.

### C. Influence of electronic correlations on the excitations

From the analysis presented above, we conclude that the lower-frequency contribution  $L_{\text{Hubbard}}$  to the mid-infrared band originates in excitations across the Mott-

Hubbard gap which allows us to determine the effective Coulomb repulsion  $U_{\text{eff}}$  to be approximately 2200 cm<sup>-1</sup>. This assignment is supported by comparing our data to spectra of the superconductor  $\kappa$ -(BEDT-TSF)<sub>4</sub>Hg<sub>2.89</sub>Br<sub>8</sub>. The replacement of the four inner sulphur atoms with selenium reduces the on-site Coulomb repulsion but increases the transfer integrals to neighboring molecules. Therefore the BEDT-TSF-based analogs are much closer to the normal metallic state; the contributions of itinerant and localized charge carriers are well separated in the optical spectra. It has clearly been observed<sup>53</sup> that with decreasing temperatures the contribution of the electrons in the conduction band (split by the Mott-Hubbard gap) shifts to lower frequencies while there is a blue shift of the excitations of the localized charge carriers. An analysis of the experimental spectra by a dimer model, which takes electron vibrational coupling into account, unambiguously allocates the 3000 cm<sup>-1</sup> band (which is weaker compared to the BEDT-TTF analogs) to intradimer transitions. It shows a very good correlation between both strength and position of the electronic excitation and emv-coupled features.

Merino and McKenzie calculated<sup>59</sup> that in strongly correlated metals the coupling between electrons and phonons leads to a non-monotonic temperature dependence of the vibrational modes near the coherence temperature  $T_{\text{coh}}$ . The shift is most pronounced (up to 5%) for phonons in the energy range comparable to  $U_{\text{eff}}/2$ , and becomes weaker for larger or smaller frequencies. Raman measurements perfectly agree with these predictions.<sup>60</sup> Of course the situation is more complicated for infrared data, because the vibrations are activated only by emv-coupling and influence in frequency and intensity by the charge excitations within the dimers. Nevertheless, this electron-phonon coupling might be an explanation for a softening of  $\nu_4(A_g)$  and  $\nu_6(A_g)$  below  $T_{\text{coh}} \approx 50$  K for the compounds  $\kappa$ -(BEDT-TTF)<sub>2</sub>Cu[N(CN)<sub>2</sub>]Br<sub>x</sub>Cl<sub>1-x</sub> with  $x = 0\%$  and 40% where the electronic correlations  $U/t$  are strongest. A close inspection reveals, that the higher frequency mode  $\nu_{45}(B_{2u})$  exhibits a similar behavior for the insulating samples with low Br content, but weaker, while no change is observed for the far-infrared vibration  $\nu_{14}(A_g)$ . This also suggests, that the effective Coulomb repulsion  $U_{\text{eff}}$  is of the order of 2000 to 2500 cm<sup>-1</sup>.

## V. CONCLUSION

Our comprehensive analysis of the temperature- and Br-concentration dependence of mid-infrared and emv-coupled features in  $\kappa$ -(BEDT-TTF)<sub>2</sub>Cu[N(CN)<sub>2</sub>]Br<sub>x</sub>Cl<sub>1-x</sub> enabled us to distinguish two contributions in the mid-infrared part of the spectra. The higher frequency  $L_{\text{dimer}}$  band (3200 cm<sup>-1</sup> for the polarization  $E \parallel c$  and presumably around 2600 cm<sup>-1</sup> for  $E \parallel a$ ) originates from the charge localized on the

BEDT-TTF dimers. This charge-transfer within the dimers is coupled to the intermolecular vibrations of BEDT-TTF and is responsible for the major part of the emv-intensity. The lower-frequency contribution to the mid-infrared band  $L_{\text{Hubbard}}$  located at  $2200 \text{ cm}^{-1}$  is isotropic and assigned to transition between two Hubbard bands which form due to strong electronic correlations. As we will show in Part II, its intensity correlates with the intensity of the Drude-peak for the metallic compounds.

## VI. ACKNOWLEDGMENTS

The authors are grateful to Alain Barreau for his help at the microscopic characterization of the sam-

ple concentrations. Belal Salameh performed the dc measurements. We acknowledge the helpful discussions with Jaime Merino and Ross McKenzie, who initiated the study many years ago. The project was partially supported by the Deutsche Forschungsgemeinschaft (DFG). ND is grateful to the Alexander von Humboldt-Foundation for the continuous support and A. Girlando, M. Masino, A. Painelli, R. Vlasova and V. Semkin for the useful discussions.

---

<sup>\*</sup> permanent address: Ioffe Physico-Technical Institute, St. Petersburg, Russia

<sup>†</sup> Electronic address: dressel@pi1.physik.uni-stuttgart.de

<sup>1</sup> D. Jérôme, in *Organic Conductors*, edited by J.-P. Farges (Marcel Dekker, New York, 1994), p. 405.

<sup>2</sup> T. Ishiguro, K. Yamaji, and G. Saito, *Organic Superconductors*, 2nd edition (Springer-Verlag, Berlin, 1998).

<sup>3</sup> R.H. McKenzie, *Science*, **278**, 821 (1997).

<sup>4</sup> H. Seo, C. Hotta, H. Fukuyama, *Chem. Rev.* **104**, 5005 (2004).

<sup>5</sup> M. Dressel and N. Drichko, *Chem. Rev.* **104**, 5689 (2004).

<sup>6</sup> T. Mori, H. Mori, and S. Tanaka, *Bull. Chem. Soc. Jpn.* **72**, 179 (1999).

<sup>7</sup> By now, the observations are not completely understood: the coupling between the layers is certainly crucial, however, simple volume effects cannot explain the behavior.

<sup>8</sup> A. Georges, G. Kotliar, W. Krauth, and M.J. Rozenberg, *Rev. Mod. Phys.* **68**, 13 (1996).

<sup>9</sup> J. Merino and R. H. McKenzie, *Phys. Rev. B* **61**, 7996 (2000).

<sup>10</sup> M. Lang and J. Müller, *Organic Superconductors*, in: *The Physics of Superconductors*, Vol. 2, edited by K.H. Bennemann and J.B. Ketterson (Springer-Verlag, Berlin, 2004), p. 453.

<sup>11</sup> K. Miyagawa, A. Kawamoto, and K. Kanoda, *Phys. Rev. Lett.* **89**, 017003 (2002).

<sup>12</sup> S. Lefebvre, P. Wzietek, S. Brown, C. Bourbonnais, D. Jérôme, C. Mzière, M. Fourmigué, and P. Batail, *Phys. Rev. Lett.* **85**, 5420 (2000).

<sup>13</sup> P. Limelette, P. Wzietek, S. Florens, A. Georges, T.A. Costi, C. Pasquier, D. Jerome, C. Meziere, and P. Batail, *Phys. Rev. Lett.* **91**, 016401 (2003).

<sup>14</sup> F. Kagawa, T. Itou, K. Miyagawa, and K. Kanoda, *Phys. Rev. B* **69**, 064511 (2004); F. Kagawa, T. Itou, K. Miyagawa, and K. Kanoda, *Phys. Rev. Lett.* **93**, 127001 (2004); F. Kagawa, K. Miyagawa, and K. Kanoda, *Nature* **436**, 534 (2005).

<sup>15</sup> J. E. Eldridge, K. Kornelsen, H. H. Wang, J. M. Williams, A. V. D. Crouch, and D. M. Watkins, *Solid State Commun.* **79**, 583 (1991).

<sup>16</sup> M. Tamura, H. Tajima, K. Yakushi, H. Kuroda, A. Kobayashi, R. Kato, and H. Kobayashi, *J. Phys. Soc. Jpn.* **60**, 3861 (1991).

<sup>17</sup> K. Kornelsen, J. E. Eldridge, H. H. Wang, H. A. Charlier, and J. M. Williams, *Solid State Commun.* **81**, 343 (1992).

<sup>18</sup> J.E. Eldridge, Y. Xie, H.H. Wang, J.M. Williams, A.M. Kini, and J.A. Schlueter, *Spectrochim. Acta A* **52**, 45 (1996); *idem*, *Mol. Cryst. Liq. Cryst.* **284**, 97 (1996).

<sup>19</sup> R.M. Vlasova, O.O. Drozdova, V.N. Semkin, N.D. Kushch, and E.B. Yagubskii, *Phys. Solid State* **38**, 481 (1996).

<sup>20</sup> J.J. McGuire, T. Rööm, A. Pronin, T. Timusk, J.A. Schlueter, M.E. Kelly, and A.M. Kini, *Phys. Rev. B* **64**, 094503 (2001)

<sup>21</sup> T. Sasaki, I. Ito, N. Yoneyama, N. Kabayashi, N. Hanasaki, H. Tajima, and Y. Iwasa, *Phys. Rev. B* **69**, 064508 (2004).

<sup>22</sup> The optical study of an alloy  $\text{BEDT-TTF})_2\text{Cu}[\text{N}(\text{CN})_2]\text{-Br}_{0.5}\text{Cl}_{0.5}$  was performed in mid-infrared and could not give an information about presence or absence of a Drude-peak.

<sup>23</sup> R.M. Vlasova, O.O. Drozdova, V.N. Semkin, N.D. Kushch, and E.B. Yagubskii, *Phys. Solid State* **35**, 408 (1993).

<sup>24</sup> O.O. Drozdova, V.N. Semkin, R.M. Vlasova, N.D. Kushch, and E.B. Yagubskii, *Synthetic Metals* **64**, 17 (1994).

<sup>25</sup> B.V. Petrov, V.N. Semkin, R.M. Vlasova, V.M. Yartsev, N.D. Kushch, and A. Graja, in: *Molecular Low-Dimensional and Nanostructured Materials for Advanced Applications*, edited by A. Graja et al. (Kluwer Academic Publ., Dordrecht, 2002), p. 259.

<sup>26</sup> K.D. Troung, B. Danilovic, D. Achkir, S. Jandl, and M. Poirier, *Synth. Met.* **85**, 1577 (1997).

<sup>27</sup> M. Dumm, D. Faltermeier, N. Drichko, M. Dressel, C. Meziere, P. Batail, J. Merino, and R. McKenzie, *to be published*

<sup>28</sup> The pure compound  $\kappa-(\text{BEDT-TTF})_2\text{Cu}[\text{N}(\text{CN})_2]\text{Cl}$  follows the rise in  $\rho(T)$  down to about 30 K, at lower temperatures the resistivity levels off at a value of approximately  $10^3 \Omega\text{cm}$  and even shows a slight drop around  $T = 10$  K. This behavior is well documented in literature<sup>29,30,31</sup> and associated with traces of superconductivity induced by internal stress or surface effects. Similar effects are seen in samples with very low Br content  $x = 15\%$ .<sup>32</sup>

<sup>29</sup> J.M. Williams, A.M. Kini, H.H. Wang, K.D. Carlson, U. Geiser, L.K. Montgomery, G.J. Pyrka, D.M. Watkins, J.M. Komers, S.J. Boryschuk, A.V. Strieby Crouch, W.K.

Kwok, J.E. Schierber, D.L. Overmyer, D. Yung, and M.H. Whangbo, *Inorg. Chem.* **29**, 3271 (1990); H.H. Wang, K.D. Carlson, U. Geiser, A.M. Kini, A.J. Schultz, J.M. Williams, L.K. Montgomery, W.K. Kwok, U. Welp, K.G. Vandervoort, S.J. Boryschuk, A.V. Strieby Crouch, J.M. Komers, D.M. Watkins, J.E. Schierber, D.L. Overmyer, D. Yung, J.J. Novoa, and M.H. Whangbo, *Synth. Met.* **41-43**, 1983 (1991).

<sup>30</sup> H. Ito, T. Ishiguro, M. Kubota, and G. Saito, *J. Phys. Soc. Jpn.* **65**, 2987 (1996).

<sup>31</sup> H. Kobayashi, A. Miyamoto, T. Naito, R. Kato, A. Kobayashi, and J.M. Williams, *Chem. Lett.* 1997 (1991).

<sup>32</sup> V.A. Bondarenko, Yu.V. Sushko, V.I. Barchuk, V.S. Yefanov, V.V. Dyakin, M.A. Tanatat, N.D. Kushch, and E.B. Yagubskii, *Synth. Met.* **56**, 2386 (1993); Yu.V. Sushko, K. Andres, N.D. Kusch, and E.B. Yagubskii, *Solid State Commun.* **87**, 589 (1993); Yu.V. Sushko, T. Ishiguro, K. Andres, S. Horiuchi, G. Saito, N.D. Kushch, and E.B. Yagubskii, *J. Supercond.* **7**, 937 (1994); H. Posselt, H. Müller, K. Andres, Yu.V. Sushko, and G. Saito, *Synth. Met.* **70**, 917 (1995).

<sup>33</sup> C.C. Homes, M. Reedyk, D.A. Cradles, and T. Timusk, *Applied Optics* **32**, 2976 (1993).

<sup>34</sup> M. Dressel and G. Grüner, *Electrodynamics of Solids* (Cambridge University Press, Cambridge, 2002).

<sup>35</sup> K. Kornelsen, J. E. Eldridge, H. H. Wang, and J. M. Williams, *Phys. Rev. B* **44**, 5235 (1992).

<sup>36</sup> J.E. Eldridge, C.C. Homes, H.H. Wang, A.M. Kini, and J.M. Williams, *Spectrochim. Acta A* **51**, 947 (1995)

<sup>37</sup> J.E. Eldridge, Y. Xie, Y. Lin, C.C. Homes, H.H. Wang, J.M. Williams, A.M. Kini, and J.A. Schlueter, *Spectrochim. Acta A* **53**, 565 (1997)

<sup>38</sup> Previously the assignment of the modes was done assuming  $D_{2h}$  symmetry of the BEDT-TTF molecule (plane BEDT-TTF molecule).<sup>5,17,18,36,37,39</sup> By now the general agreement is that the molecules in  $\kappa$ -(BEDT-TTF)<sub>2</sub>Cu(NCS)<sub>2</sub> only have  $D_2$  due to the twisted ethylene groups<sup>40,41,42</sup> leading to 19  $A_1$  totally symmetric modes. For the  $\kappa$ -(BEDT-TTF)<sub>2</sub>Cu[N(CN)<sub>2</sub>]Br and  $\kappa$ -(BEDT-TTF)<sub>2</sub>Cu[N(CN)<sub>2</sub>]Cl-family the molecules are eclipsed and exhibit only  $C_{2h}$  symmetry, as recently pointed out in Ref. 43.

<sup>39</sup> M.E. Kozlov, P.I. Pokhodnia, and A.A. Yurchenko, *Spectrochim. Acta A* **43**, 323 (1987); M.E. Kozlov, P.I. Pokhodnia, and A.A. Yurchenko, *Spectrochim. Acta A* **45**, 437 (1989).

<sup>40</sup> M. Meneghetti, R. Bozio, and C. Pecile, *J. Phys. I (France)* **47**, 1377 (1986); *Synth. Met.* **19**, 143 (1987).

<sup>41</sup> A. Girlando, M. Masino, A. Brillante, R.G. Della Valle, and E. Venuti, to be published in: *Horizons in Superconductivity Research* (Nova Science Publisheres, New York, 2004).

<sup>42</sup> J. M. Williams, J. R. Ferraro, R. J. Thorn, K. D. Carlson, U. Geiser, H. H. Wang, A. M. Kini, and M. H. Whangbo, *Organic Superconductors* (Prentice Hall, Englewood Cliffs NJ, 1992).

<sup>43</sup> R. Wesolowski, J.T. Haraldsen, J. Cao, J.L. Musfeldt, I. Olejniczak, J. Choi, Y.J. Wang, and J.A. Schlueter, *Phys. Rev. B* **71**, 214514 (2005).

<sup>44</sup> T. Sugano, H. Hayashi, M. Kinoshita, and K. Nishikida, *Phys. Rev. B* **39**, 11387 (1989).

<sup>45</sup> M.J. Rozenberg, G. Kotliar, H. Kajueter, G.A. Thomas, D.H. Rapkine, J.M. Honig, and P. Metcalf, *Phys. Rev. Lett.* **75**, 105 (1995); M.J. Rozenberg, G. Kotliar, H. Kajueter, *Phys. Rev. B* **54**, 8452 (1996).

<sup>46</sup> R.H. McKenzie, *Comments Cond. Mat.* **18**, 309 (1998).

<sup>47</sup> D. Jung, M. Evain, J.J. Novoa, M.H. Whangbo, M.A. Beno, A.M. Kini, A.J. Schultz, J.M. Williams and P.J. Nigrey, *Inorg. Chem.* **28**, 4516 (1989).

<sup>48</sup> U. Geiser, A.J. Schultz, H.H. Wang, D.M. Watkins, D.L. Stupka, J.M. Williams, J.E. Schirber, D.L. Overmyer, D. Jung, J.J. Novoa and M.H. Whangbo, *Physica C* **174**, 475 (1991).

<sup>49</sup> H. Kino and H. Fukuyama, *J. Phys. Soc. Jpn.* **64**, 2726 (1995); *ibid.* **64**, 4523 (1995); *ibid.* **65**, 2158 (1996).

<sup>50</sup> K. Kanoda, *Hyperfine Interact.* **104**, 235 (1997).

<sup>51</sup> A. Fortunelli and A. Painelli, *Phys. Rev. B* **55**, 16088 (1997).

<sup>52</sup> By comparing the effects of 'chemical' and hydrostatic pressure, Mori *et al.*<sup>6</sup> point out that the application of the hydrostatic pressure (but also thermal contraction) to the Cl compound reduces the b1/p ratio, leading a less correlated state.

<sup>53</sup> R.M. Vlasova, N.V. Drichko, B.V. Petrov, V.N. Semkin, E.I. Zhilyaeva, R.N. Lyuboskaya, I. Olejniczak, A. Kobayashi, and H. Kobayashi, *Phys. Solid State* **46**, 1985 (2004); N. Drichko, B. Petrov, V.N. Semkin, R.M. Vlasova, O.A. Bogdanova, E.I. Zhilyaeva, R.N. Lyuboskaya, I. Olejniczak, H. Kobayashi, and A. Kobayashi, *J. Phys. IV (France)* **114**, 305 (2004).

<sup>54</sup> As discussed in the following paragraph, the  $\nu_4$  mode appears as a double peak due to the  $\nu_6$  antiresonance. We fit the complete feature by a Lorentzian and choose the center frequency, while commonly the upper peak is listed as the  $\nu_4$  frequency.

<sup>55</sup> M.J. Rice, *Phys. Rev. Lett.* **37**, 36 (1976).

<sup>56</sup> V.M. Yartsev, O.O. Drozdova, V.N. Semkin and R.M. Vlasova, *J. Phys. I (France)* **6**, 1673 (1996); V.M. Yartsev, in: *Materials and Measurements in Molecular Electronics*, ed. by K. Kajimura and S. Kanoda (Springer-Verlag, Berlin 1996), p. 189; V. M. Yartsev and A. Graja, *Int. Journ. of Mod. Phys. B*, **12**, 1643 (1998).

<sup>57</sup> V. M. Yartsev, O. Fichet, J.-P. Borgion and P. Dehaes, *J. Phys. II France* **3**, 647 (1993)

<sup>58</sup> G. Visentini, M. Masino, C. Bellitto, and A. Girlando, *Phys. Rev. B* **58**, 9460 (1998).

<sup>59</sup> J. Merino and R. H. McKenzie, *Phys. Rev. B* **62**, 16442 (2000).

<sup>60</sup> Y. Lin, J.E. Eldridge, H.H. Wang, A.M. Kini, M.E. Kelly, J.M. Williams, and J.A. Schlueter, *Phys. Rev. B* **58**, R599 (1998).